ISSN 0010-5082, Combustion, Explosion, and Shock Waves, 2021, Vol. 57, No. 5, pp. 521–536. © Pleiades Publishing, Ltd., 2021.
Russian Text © E.P. Mitsopoulos, P. Koutmos, E. Manouskou, I. Georgantas.

# Reduced Kinetic Model for Complex Turbulent *n*-Heptane Flame Simulations

**E. P. Mitsopoulos[a], P. Koutmos[a], E. Manouskou[a], and I. Georgantas[a]**

UDC 536.46+662.12

Published in *Fizika Goreniya i Vzryva*, Vol. 57, No. 5, pp. 14–30, September–October, 2021.
Original article submitted October 20, 2020; revision submitted October 20, 2020; accepted for publication February 19, 2021.

**Abstract:** In large-scale turbulent flame simulations, the exploitation of detailed chemistry and transport models often necessitates expensive memory and CPU requirements. To maintain the practicality and flexibility of such simulations, the combustion chemistry is commonly represented by reduced reaction mechanisms. The present paper describes the development of such a reduced short kinetic scheme for high-temperature oxidation of *n*-heptane suitable for application in complex turbulent flame simulations. Through a combination of the directed relation graph and quasi-steady state approximation methodologies, a skeletal 65-species kinetic model is formally reduced down to a 25-species derivative suitable for atmospheric lean to stoichiometric conditions. Further removal of appropriate reactions and species is facilitated by using the reaction path flux analysis, yielding a short chemical scheme of 25 species and 69 reactions. Particular attention is given to avoid addition of lumped reactions (for all isomer compounds) and artificial kinetic rates expressed as nonlinear algebraic combinations of excluded elementary steps. In addition, most of the original radical reaction pathways are duly preserved, and an adequate number of intermediate lighter-chain hydrocarbon species is represented in the reduced scheme to ensure a proper breakdown and oxidation of the main hydrocarbon. A series of 0D and 1D propagating and counterflowing premixed flames and axisymmetric coflowing laminar jet flames are computed throughout an iterative validation procedure. Complementary computations with the 65-species base scheme, as well as available experimental data are exploited for the assessment of the optimization effort. The comparisons demonstrate that the derived scheme ensures satisfactory agreement with these data over the investigated parameter space.

*Keywords*: reduced combustion chemistry, *n*-heptane oxidation, laminar flames, chemical reaction schemes.

**DOI:** 10.1134/S0010508221050026

## INTRODUCTION

Novel combustion technologies with lower emissions, higher efficiencies, and wider fuel flexibility have become essential in the design of new combustion devices in the effort to address environmental concerns and energy supply challenges. Industrial burners and propulsion devices are fed with liquid fuels and operate with very strong interactions between turbulence, combustion, spray, evaporation, heat transfer, and radiation within the combustion chamber. Profound understanding and optimization of such complex processes necessitates the exploitation of multi-scale simulations as an adjunct to laboratory tests [1–4].

Developments in large-eddy simulations (LES) made it possible to investigate the processes in turbulent reacting flows in laboratory [2] or industrial configura-

[a]Laboratory of Applied Thermodynamics, Department of Mechanical Engineering and Aeronautics, University of Patras, Patras, 26504 Greece; epmitsopoulos@gmail.com.

tions (e.g., [5]) with convincing success. In advanced combustors, adequate modelling of the multi-physics nature of spray, radiation, pollutant emissions, auto-ignition, flame propagation, and flash-back requires consideration of the broad range of fluid and chemical length and times scales involved (see [1]). This entails the adoption of sufficiently detailed, but tractable chemistry and transport models [6, 7]. Integrating the combustion chemistry within LES involves finding suitable reaction mechanisms and solving filtered equations for each individual species appearing in the reaction mechanism. The latter may involve dozens of species and hundreds of reactions leading to prohibitive requirements to computer resources. Therefore, reduced chemical schemes were suggested as an affordable alternative within the Reynolds-averaged Navier–Stokes (RANS) or LES procedures [4, 8].

Several strategies were put forward to reduce a detailed mechanism as discussed in [6, 9]. Starting with a comprehensive chemistry library (see, e.g., [10]), the first level of simplification through identification and elimination of elementary reactions and redundant species can be undertaken by applying the optimized directed relation graph (DRG) methodology, possibly, in combination with the sensitivity analysis approach [6, 9, 11]. Further reduction of the skeletal mechanism can be carried out by revoking a combination of quasi-steady state assumptions for species and partial equilibrium for reactions using, e.g., the quasi-steady state approximation (QSSA) [12], the computational singular perturbation (CSP) [6, 11], the chemical lumping method [13], or the ACR method [14]. For different degrees of desired accuracy and speed, these procedures can provide varying levels of mechanism reduction and complexity.

In cases of very complex simulations, even global chemistry descriptions representing kinetic models with fitted chemical parameters that are developed through calibration procedures are tolerable. Quasi-global kinetic models retain a sub-set of the original mechanism, such as, e.g., the $H_2$–$O_2$/CO system, and employ one or more global fuel decomposition steps with rates calibrated over a range of targeted conditions (see, e.g., [8]). The challenge in providing a useful kinetic description is to select accurate representations of the major ignition steps, rate parameter adaptations, and suitable global reactions; by nature, these schemes are constrained to smaller molecules and a narrow range of conditions [8, 15].

Within this context, the intention of the present effort was to develop a reduced and tractable 25-species chemical model for high-temperature oxidation of *n*-heptane. The base mechanism from which this was deduced was a 65-species, 315-reaction scheme for *n*-$C_7H_{16}$/air [16]. The motivation here was to bridge the gap between extended mechanisms involving a significant number of species and reactions and quasi-global models utilizing, e.g., less than 10 species [8, 15].

*n*-Heptane is the hydrocarbon that exhibits chemical properties, laminar flame speeds, and extinction behavior that are comparable to those of heavier paraffin fuels used in practical engine operation. Alone or in surrogate mixtures, *n*-heptane is considered as a viable laboratory-scale substitute for commercial diesel fuels, as well as gasoline fuels. For example, a mixture of *n*-heptane with iso-octane constitutes the primary reference fuel (PRF) mixture for gasoline [17]. If toluene is added to the mixture, the surrogate blend of *n*-heptane, iso-octane, and toluene (TPRF) expands its usefulness in modelling an even wider range of liquid fuels with varying octane sensitivity [18]. This aspect makes *n*-heptane attractive as a model fuel for a range of experimental and computational studies of internal combustion engines.

The present effort is also directly connected to an extension of previous studies of the characteristics of gaseous, stratified, turbulent bluff-body flames (see, e.g., [19, 20]) to heavier liquid fuels of more direct significance to engine applications. The intention is to exploit the derived simplified shorter flexible kinetic model and enlarge the scope of LES simulations of the laboratory-scale recirculating flames. Consequently, the simplified *n*-heptane high-temperature scheme is specifically aimed at atmospheric flames and lean to near-stoichiometric equivalence ratios between 0.55 and 1.3. Nevertheless, its applicability can be expanded through possible developments and extensions. The chemical parameters of this scheme are tuned by reference to the 65-species scheme and available experimental data. Validation runs are assessed for equilibrium calculations and auto-ignition delay times in 0D flames, 1D freely propagating and counterflowing premixed flames, and 2D coflowing laminar jet flames, both lifted and attached.

## 1. DESCRIPTION OF DERIVATION OF SIMPLIFIED REDUCED MODELS

### *1.1. Formulation and Objectives of Reduction Effort*

The motivation here is to produce a simplified reduced kinetic model for *n*-heptane that can be productively exploited in reactive simulations of practical complexity. The significant species and reactions retained in this scheme are targeted, on the one hand, on reproduction of the performance of larger schemes in lami-

List of species in two schemes employed in the present study

| Number of species | List of species |
|---|---|
| 65 | H, O, OH, $HO_2$, $H_2$, $H_2O$, $H_2O_2$, $O_2$, CH, $CH_2$, $CH_2^*$, $CH_3$, $CH_4$, HCO, $CH_2O$, $CH_3O$, $CH_2OH$, $CH_3OH$, CO, $CO_2$, $C_2H$, $C_2H_2$, $C_2H_3$, $C_2H_4$, $C_2H_5$, $C_2H_6$, HCCO, $CH_2CO$, $CH_3CO$, $CH_2CHO$, $CH_3CHO$, $C_3H_3$, *p*-$C_3H_4$, *a*-$C_3H_4$, *a*-$C_3H_5$, $CH_3CCH_2$, $C_3H_6$, *n*-$C_3H_7$, *i*-$C_3H_7$, $C_2H_3CHO$, $C_4H_2$, *i*-$C_4H_3$, $C_4H_4$, *i*-$C_4H_5$, $C_4H_5$-2, $C_4H_6$, $C_4H_6$12, $C_4H_6$-2, $C_4H_7$, $C_4H_8$1, *p*-$C_4H_9$, $NC_7H_{16}$, $PXC_7H_{15}$, $SXC_7H_{15}$, $C_7H_{14}$, $C_7H_{13}$, $PXC_6H_{13}$, $PXC_5H_{11}$, $SXC_5H_{11}$, $C_5H_{10}$, $C_5H_9$, $S2XC_7H_{15}$, $S3XC_7H_{15}$, $S2XC_5H_{11}$, $N_2$ |
| 25 | H, O, OH, $HO_2$, $H_2$, $H_2O$, $O_2$, $CH_2$, $CH_2^*$, $CH_3$, $CH_4$, HCO, $CH_2O$, CO, $CO_2$, $C_2H_2$, $C_2H_3$, $C_2H_4$, $C_2H_5$, *a*-$C_3H_5$, $C_3H_6$, *p*-$C_4H_9$, $NC_7H_{16}$, $SXC_7H_{15}$, $N_2$ |

nar prototype flames and, on the other hand, on the improved prediction of different experimental behaviors obtained in lean to near-stoichiometric premixed and stratified turbulent flames.

Particular attention is paid to the ability of the scheme to represent optical measurements, such as spatially resolved laser-induced fluorescence (LIF), chemiluminescence, heat release signatures, as well as temperature and pollutant profiles. The effort is also aimed at reproduction of limiting phenomena, such as local extinctions, flash-back, and lean blow-off. To that end, the 25-species model retains minor species, radicals, and intermediate hydrocarbons that are deemed necessary for the appropriate calculation of the above-mentioned parameters.

### *1.2. Reduction and Simplification Methodologies Applied*

The chemistry set employed in this work was based on the skeletal kinetic model of Smallbone et al. [16], which comprised 65 species and 315 reactions. This scheme has been widely tested against experimental results for laminar flame speeds and counterflow flames over equivalence ratios from 0.7 to 1.4 and low pressures (0.5 to 2 atm).

Within the present effort, starting from the 65-species scheme, the reduction and simplification process was directed at producing a simplified kinetic model for lean to near-stoichiometric mixtures ($\phi = 0.55-1.3$) and high-temperature oxidation at atmospheric conditions. The list of species retained in the present scheme is shown in the table, whilst the details of the 25-species scheme are presented in the Appendix.

In the 65-species scheme, the major fuel consumption steps are thermal decomposition and H and OH attack, leading to H abstraction and to intermediate heptyl isomers. Products of the alkyl decomposition steps higher than $C_3$ also undergo fast thermal decompositions and form $C_3$ and $C_2$ species with ethene ($C_2H_4$) and propene ($C_3H_6$) being the important stable ones. Propene reacts with H radicals to form propyl (*n*-$C_3H_7$) and subsequently decomposes to form ethene and methyl. Ethene follows the $C_2$-chain to $C_2H_3$, $CH_3$, and $C_2H_2$ mainly through reactions with H and OH. Oxidation of the $C_1$ and $C_2$ chains follows the route of smaller fuel molecules, such as methane.

A further formal reduction of the skeletal 65-species scheme through application of systematic DRG and combined species sensitivity analysis and time scale identification based on the level of importance (LOI) parameter [13] was applied, while observing the introduced errors with respect to reproduction of key metrics such as flame speeds, ignition delays, and major species and radical concentrations. The goal here is to deduce a still smaller mechanism, with fewer transported species and lower chemical stiffness to enable significant savings in the CPU time and memory in large-scale computations. This obviously would entail a tradeoff between the size, accuracy, and universality of application in different flames in the resulting simplified model. The aim in this shorter scheme is also to avoid rate parameters being expressed in terms of linear algebraic combinations of the excluded elementary step rates, e.g., as pursued in [12]. Specifically, the DRG with the error propagation methodology was followed, as implemented through the Chemkin software [21], to eliminate any low-importance species within the targeted lean-to-stoichiometric low-pressure conditions. This effort yielded a reduced scheme with 35 species and 200 reactions, whilst the errors incurred in the performance metrics were augmented, but still remained within the preset limits. Nevertheless, a still shorter, more flexible model was attempted by implementing the full species sensitivity analysis (FSSA) approach, reaching a set with 25 species and 105 reactions. Here the final choice for species retention was also governed by the intention to facilitate comparisons between 3D turbulent simulations and experimental data related to optical imaging techniques. For instance, the major

radicals or species associated with kinetic models employed for calculating chemiluminescence, such as, e.g., $C_2H_2$, CHO, and $CH_2$ [22] were specifically retained in the proposed models, whereas a number of intermediate hydrocarbon species were omitted due to their limited impact on the laminar flame speed and ignition delay time. Nevertheless, many of more important intermediates, such as $C_3H_6$, $C_4H_9$, and $C_3H_5$, were retained to preserve the accuracy of the main hydrocarbon oxidation pathway. The combination of a suitably tailored shorter scheme with an extended or simplified kinetic model for chemiluminescence (e.g., [22, 23]) will broaden the scope of direct comparisons between measurements and large-scale simulations [24]. Successively, by utilizing the reaction path analysis, the prevalent consumption and production pathways, based on their respective rates of production, were identified for each of the remaining 25 species. Accordingly, a further 36 reactions were removed, yielding the final scheme with 25 species and 69 reactions. Again, particular emphasis was paid to preserve the major radical reaction pathways, with many of the omitted reactions originating from the intermediate hydrocarbon pool. The resulting reduced mechanism, as expected, exhibits in certain cases a different behavior than the base 65-species set. The omission of species and reactions has a somewhat unfavorable effect on the accuracy of the deduced mechanisms; therefore, a systematic effort was undertaken to compensate for this through targeted modifications and tuning of constants in a few selected reactions. This approach has been previously followed by various researchers (e.g., [25]). This may somewhat restrict the range of application of the derived model, restricting its optimum application within a narrower parameter space, as was noted above. The omitted species can be found in the table.

### *1.3. Reduced Model Mechanism Tuning and Validation Procedure*

Agreement between the simplified and the starting mechanisms is assessed based on the reproduction of several prime performance indicators considered as correct target measures. Adiabatic temperatures, species distributions, autoignition times, flame speeds, and extinction strain rates were computed in equilibrium 0D and 1D propagating premixed flames over a range of conditions. The model performance was also examined in configurations encountered in practical combustion arrangements, such as non-premixed lifted laminar jet flames. Associated computations with the 65-species mechanism, as well as experimental data and computations reported in the literature, were exploited as optimization targets.

The subsequent iterative manual regression process was made tractable by the relatively narrow parameter space covered by the reduced 25-species scheme. Therefore, it was possible to focus on a small number of reactions selected on the basis of the sensitivity analysis and the rate of production. The tuning and calibration process focused more on fitting of the pre-exponential values of intermediate hydrocarbons and less on the major radical production pathways. The main hydrocarbon reaction with the H and O radicals was tuned to balance the ignition delay times (see reaction Nos. 66 and 67 in Appendix), whereas the $C_3H_6$ consumption pathways with H (reaction Nos. 59 and 60) were tuned to improve the laminar flame speeds of the lean-to-stoichiometric mixtures. Then the reaction rates of the ethyl radical with H to $C_2H_4$ (reaction No. 53), as well as the consumption of $C_2H_4$ with O to $CH_3$ and HCO (reaction No. 50) were calibrated to accomplish better prediction of $C_2H_4$ concentrations in the reference counterflow flame configuration. The consumption of $C_2H_3$ with H towards $C_2H_2$ (reaction No. 43) was proven to be critical in the correct prediction of laminar flame speeds in the lean branch. Finally, the concentration of the $CH_4$ species in the counterflow configuration was significantly affected by the reaction of $CH_4$ with OH towards $CH_3$ (reaction No. 40).

All of the parametric 0D and 1D kinetic simulations used to verify the performance of the reduced scheme against the selected target data were completed utilizing the Chemkin software [21]. The lifted flame configuration was computed utilizing the ANSYS software, Realise 19 [26] employing its laminar stiff chemistry and direct kinetics solver. The axisymmetric mesh used for both the 65-species scheme, used as target data, as well as the reduced 25-species scheme comprised 178 000 nodes spanning 80 fuel nozzle diameters in the axial direction and 20 fuel nozzle diameters in the radial direction. This geometry was employed in the experiments of Toma et al. [27] and was reproduced in the simulations along with the experimental inlet velocities, mixture fractions, and boundary conditions. A zero radial velocity and a zero gradient for the axial velocity, temperature, and species concentrations were assumed on the axis and the open boundaries, whilst a zero gradient was applied at the outflow. Any significant discrepancies identified in these 2D test runs led to modest readjustment of the intermediate hydrocarbon consumption and production rate parameters in the model schemes, and these changes were, in turn, fed back to the 1D flame calibration runs. This iterative cycle produced the final tuned set of the kinetic rate parameters (see Appendix).

## 2. VALIDATION OF SIMPLIFIED REDUCED KINETIC MODELS, RESULTS AND DISCUSSION

The performance of the simplified high-temperature oxidation model was first evaluated by computing the auto-ignition delay times of stoichiometric *n*-heptane/air mixtures at $p = 1.0$, 3.2, and 6.5 bars. The initial auto-ignition temperatures were in the range of 1100–2000 K, avoiding the implication of the low-temperature oxidation behavior, which is not represented in the present scheme. Calculations for those stoichiometric mixtures in the above-stated pressures were obtained with the 65- and 25-species schemes and are shown in Fig. 1. Those results were validated against experiments reported by Ciezki and Adomeit [28] for the $p = 3.2$ and 6.5 bar cases. Adequate reproduction of ignition delay times is directly related to the ability of a scheme to predict transient combustion processes, such as ignition and extinction. Success in this respect necessitates a good representation of primary radicals, such as O, H, OH, and $HO_2$, an aspect that has been addressed in the 25-species model. These comparisons indicate that the present reduced scheme follows satisfactorily the trend and the quantitative range of the target data including that of the 65-species scheme. Tuning of the pre-exponential factor of the HCO breakdown reactions (reaction Nos. 19 and 21), as well as that of the $C_3H_6$ consumption by H (reaction No. 60) proved to be critical in attaining the above-mentioned agreement between the two kinetic schemes.

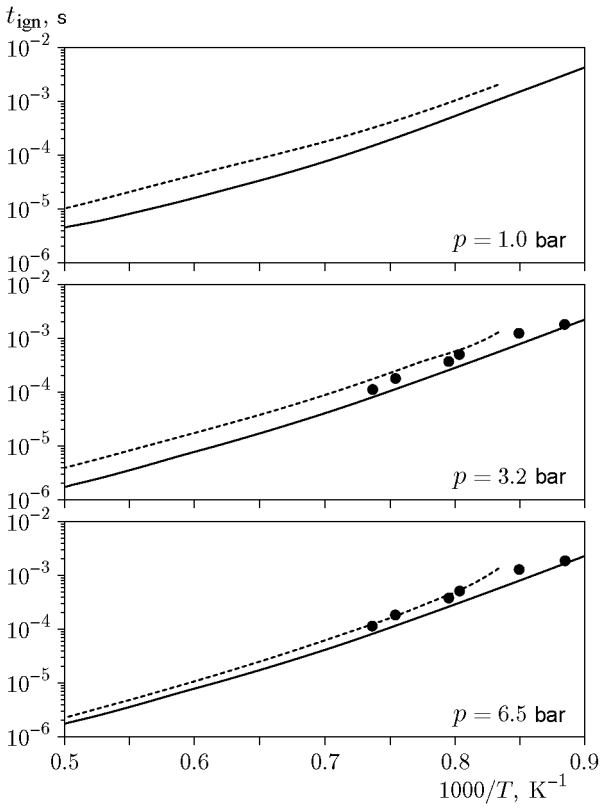


**Fig. 1.** Auto-ignition delay times predicted for stoichiometric mixtures for different pressures: the solid and dashed curves show the results computed with the 65-species scheme and with the present 25-species scheme, respectively; the points refer to the experimental data [28].

The performance of the reduced scheme was subsequently tested by calculating unstretched laminar flame speeds in adiabatic or preheated freely propagating 1D flames for various equivalence ratios $\phi$ and comparing the results against experimental data and the 65-species mechanism. As the flame speed corresponds to a global parameter that accounts for the diffusivity, exothermicity, and reactivity of the mixture, its accurate reproduction over a range of $\phi$ represents a stringent test.

Comparisons of the predicted flame speeds for various equivalence ratios, inlet temperature levels, and pressures are illustrated in Fig. 2. The predicted lean and stoichiometric part of the curve appears quite satisfactory with a peak deviation of 10% with respect to experimental values and the 65-species scheme. Those deviations become greater as the mixtures exceed the equivalence ratio of 1.1, a behavior clearly observed over the preheat and pressure fields presented. This can be attributed to the omission of important intermediate secondary hydrocarbons in the initial fuel oxidation route. Nonetheless, the performance of the reduced scheme is seemingly equivalent to that of the 65-species scheme, owing to the targeted fitting procedure of the selected pre-exponential constants.

In Fig. 3, the extinction strain rate ($\alpha$) computed by the 65-species skeletal scheme for the configuration of Ji et al. [29] is compared against that produced by the reduced 25-species scheme and the experimental results. Ji et al. [29] employed a counterflow configuration of two impinging jets, one supplying fully premixed *n*-heptane/air mixtures with varying equivalence ratios at 353 K, and the opposite supplying the nitrogen gas at 300 K. Again, the deviations between the reduced and the 65-species schemes are within 10% in the lean and near-stoichiometric regions $\phi \leqslant 1$. This deviation becomes more pronounced in the richer region, beyond equivalence ratios of around $\phi > 1.1$.

Amongst various configurations used here as target flames, a 1D stretched laminar premixed flame formed through two opposed fuel jets was also studied. Specifically, partially premixed *n*-heptane flames produced by

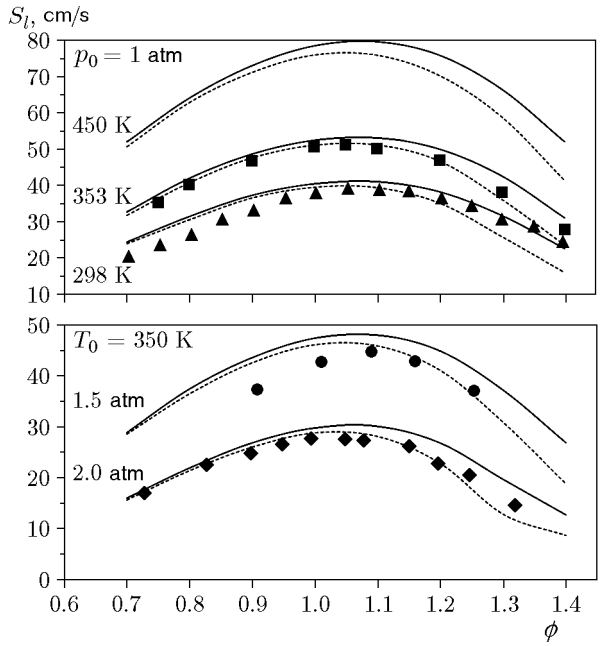


**Fig. 2.** Laminar flame speed for freely propagating premixed flames for different initial temperatures and pressures: the solid and dashed curves show the results computed with the 65-species scheme and with the present 25-species scheme, respectively; the points are the experimental data obtained in [16] (▲ and ●), [29] (■), and [16] with dilution by nitrogen (◆).

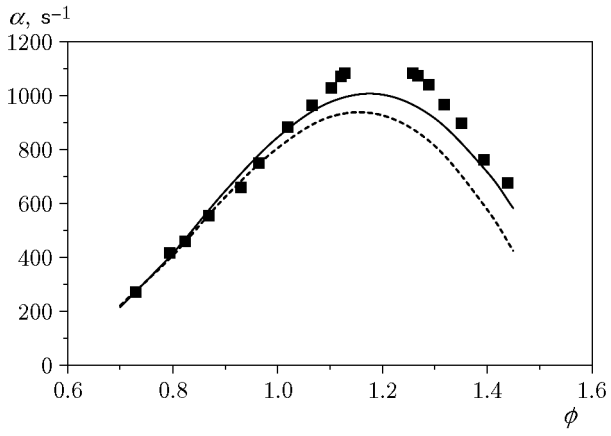


**Fig. 3.** Extinction strain rates for $n$-$C_7H_{16}$/air flames for $T_0 = 353$ K and $p_0 = 1$ atm: the solid and dashed curves show the results computed with the 65-species scheme and with the present 25-species scheme, respectively; the points refer to the experimental data [29].

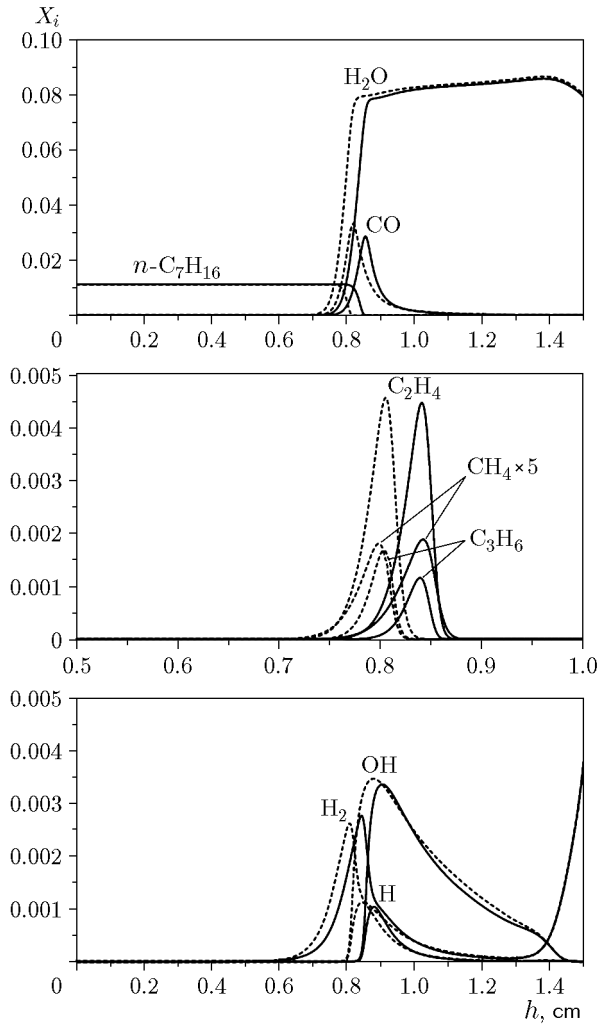


**Fig. 4.** Species distributions for a lean ($\phi = 0.6$) Cheng-type counterflow configuration [30]: $L = 15$ m, $T_0 = 400$ K, $p_0 = 1$ atm, oxidizer-side equivalence ratio $\phi = 0.28$ in the $O_2/H_2$ mixture, and $T_0 = 300$ K; the solid and dashed curves show the results computed with the 65-species scheme and with the present 25-species scheme, respectively.

counterflowing reactant jets of disparate and very lean or rich stoichiometry, i.e., a lean $H_2$/air jet impinging against near-stoichiometric or lean $n$-$C_7H_{16}$/air jets, were computed. The experimental study of such configurations has already proven useful for propane flames (e.g., [30]), since these are of direct relevance to stratified operation of either direct injection spark ignition engines or practical bluff body or swirl flame stabilizers; therefore, these were exploited in the present tests as well.

Here, in a fashion similar to that in the study of Dogkas et al. [31], two flames formed by an $n$-$C_7H_{16}$/air jet opposing hot products from an $H_2$/air jet with

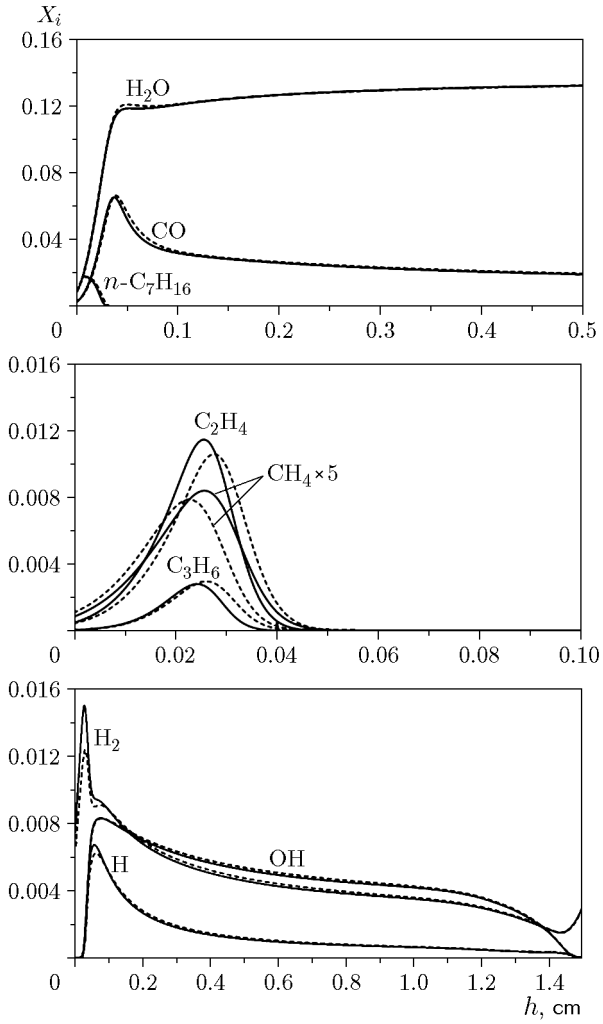


**Fig. 5.** Species distributions for a stoichiometric ($\phi = 1.0$) Cheng-type [30] counterflow configuration: $L = 15$ mm, $T_0 = 400$ K, $p_0 = 1$ atm, oxidizer-side equivalence ratio $\phi = 0.28$ in the $O_2/H_2$ mixture, and $T_0 = 300$ K; the solid and dashed curves show the results computed with the 65-species scheme and with the present 25-species scheme, respectively.

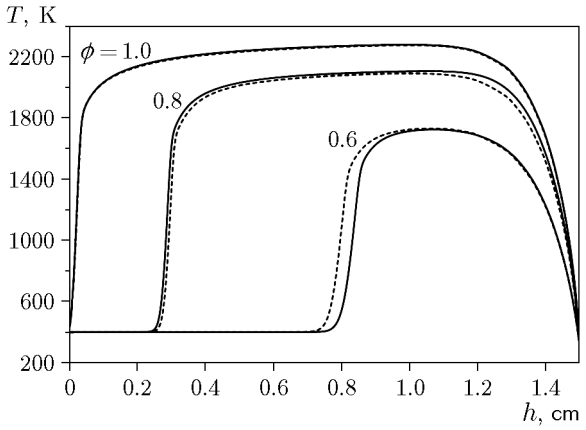


**Fig. 6.** Temperature distributions for a Cheng-type [30] counterflow configuration: $L = 15$ mm, fuel-side equivalence ratio $\phi = 0.6$, 0.8, and 1.0, $T_0 = 400$ K, $p_0 = 1$ atm, oxidizer-side equivalence ratio $\phi = 0.28$ in the $O_2/H_2$ mixture, and $T_0 = 300$ K; the solid and dashed curves show the results computed with the 65-species scheme and with the present 25-species scheme, respectively.

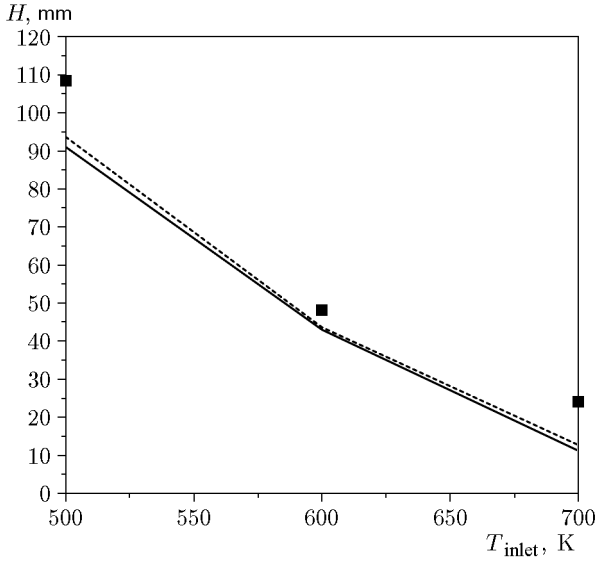


**Fig. 7.** Flame lift-off height over the burner: the solid and dashed curves show the results computed with the 65-species scheme and with the present 25-species scheme, respectively; the points are the experimental data [27]; the jet velocity is 1.5 m/s, the coflow velocity is 0.4 m/s, and the *n*-heptane mole fraction is 0.035.

$\phi = 0.28$ at a strain rate $\alpha = 140$ s$^{-1}$ were computed; the first one was an $n$-$C_7H_16$/air mixture at $\phi = 1$, and the second one was an ultra-lean, near-limit configuration with $\phi = 0.6$. Comparisons between the computed temperatures, major and minor species, and radicals with the present simplified scheme and the 65-species scheme are shown in Figs. 4–6.

The results from the limiting flame computation at $\phi = 0.6$ are displayed in Fig. 4. The ($X_i$) CO, $H_2O$, and $n$-$C_7H_{16}$ profiles, as well as those of the intermediate hydrocarbons and radicals, are reproduced well, despite reverting to a mixture that is at the lean flammability limit (simply sustained by the hydrogen stream).

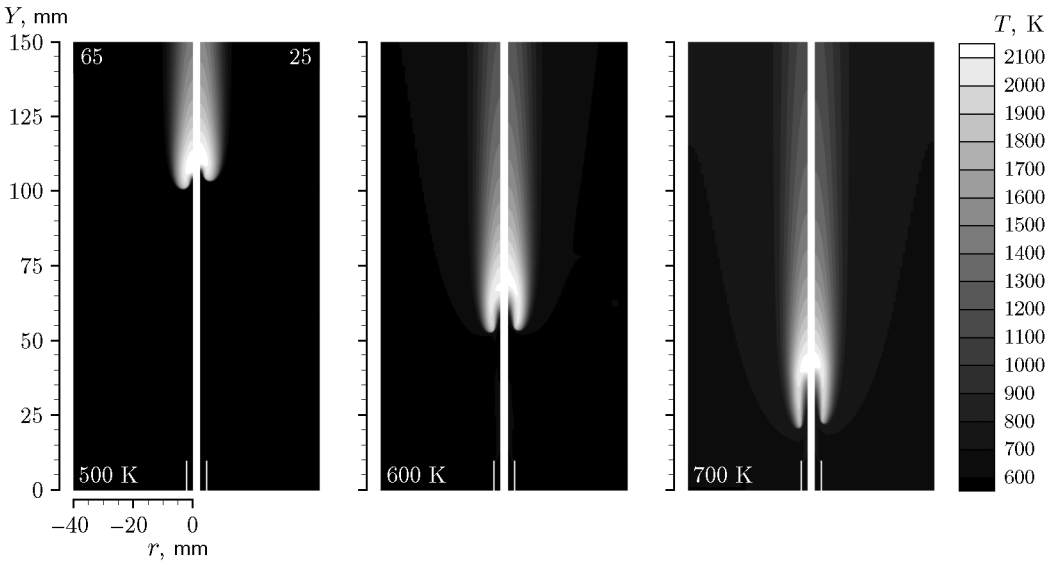


**Fig. 8.** Simulation of the lifted flame temperature fields with the reference scheme (65 species) and reduced scheme(25 species) for $T_0$ = 500, 600, and 700 K (the jet velocity is 1.5 m/s, the coflow velocity is 0.4 m/s, and the *n*-heptane mole fraction is 0.035).

A slight shift of the flame front in the reduced scheme toward the $H_2$/air side can be noticed in the species profiles, probably due to weaker penetration of the flame into the *n*-heptane/air mixture. This cannot be directly traced to a lower propagation speed since this is rather well predicted over this specific $\phi$ region. The successful representation of these complex flame patterns lends further credibility to the proposed scheme. It decidedly reflects their ability to study behaviors related to ignition, extinction, and flashback in practical laboratory flames [24, 25]. Furthermore, the adequate representation of both $C_2H_2$ and important radicals is very encouraging, since direct correlations between 3D simulations and chemiluminescence optical images exploit global kinetic sub-models relying on such species (e.g., [22, 23]).

As shown in Fig. 5, the simplified scheme also reproduces well the major and minor species profiles in the stoichiometric flame studied. A slight shift of the flame front towards the $H_2$/air side is again notable in the species profiles, albeit less pronounced. It could be argued that the reduced scheme exhibits more pronounced differences compared to the 65-species scheme, closer to extinction than in the more stable counterflow configuration with $\phi = 1$. This argument is further supported by the temperature profiles of the counterflow configuration plotted in Fig. 6 for the two schemes. The temperature plateau is slightly wider for the limiting $\phi = 0.6$ flame, a trend that becomes weaker as we progress towards stoichiometric mixtures.

Subsequently a range of axisymmetric coflowing lifted laminar jet flames were calculated, targeting the qualitative and quantitative reproduction of the temperature, major species fields, and lift-off heights. These represent a severe test of the reduced scheme's ability to capture complex flame structure features that are more frequently encountered in practical configurations. The axisymmetric burner geometry utilized for the present simulations was described in detail by Toma et al. [27]. It includes a central fuel jet with an internal diameter of 3.76 mm and a surrounding annular air coflow with and internal diameter of 130 mm. Those dimensions were also maintained for the domain used to carry out the simulations. The variations in the lift-off characteristics of these flames were investigated by changing the inlet temperature of the fuel air stream between 500 and 700 K. The following test case parameters were used: fuel inlet bulk velocity 1.5 m/s, air coflow bulk velocity 0.4 m/s, and constant fuel mixture composition kept at 0.035/0.965 $n$-$C_7H_{16}/N_2$ mole fraction. A fuel inlet temperature variation resulted in a variety of stable attached or lifted flames. The commercial software ANSYS Fluent [26] was used to perform these computations as discussed in Section 1.3.

The lift-off height $H$ of each flame is shown in Fig. 7 for the 65-species and 25-species schemes together with the experimental data obtained by Toma et al. [27]. It should be noted that the lift-off height of each flame presented is the distance between the fuel nozzle exit

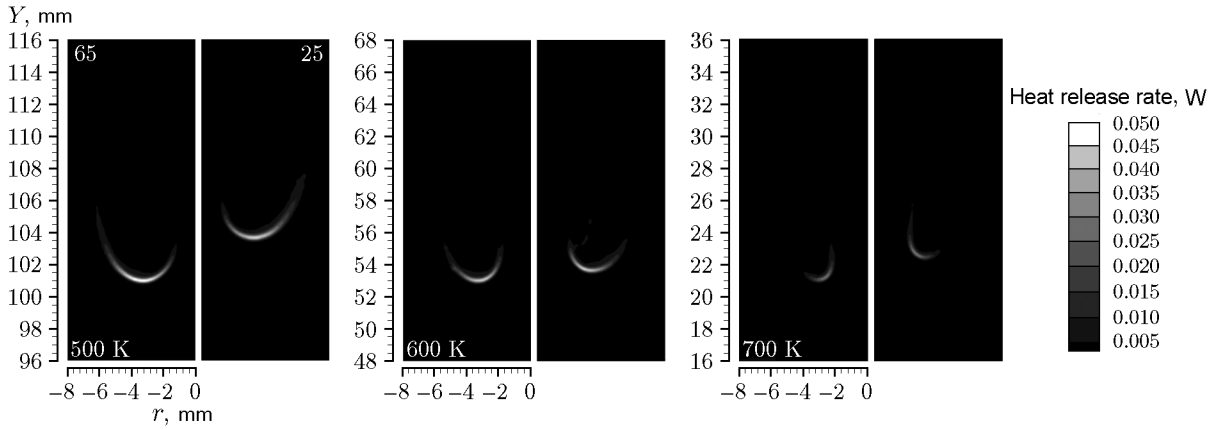


**Fig. 9.** Simulation of the heat release rate fields with the reference scheme (65 species) and reduced scheme (25 species) for $T_0 = 500$, 600, and 700 K (the jet velocity is 1.5 m/s, the coflow velocity is 0.4 m/s, and the *n*-heptane mole fraction is 0.035).

plane and the flame attachment position. Good agreement between the reduced 25-species scheme and the reference 65-species scheme is observed for all the fuel stream preheat cases studied. The decreasing trend of the lift-off height with increasing fuel inlet temperatures is very well captured, albeit with a peak deviation of 10% observed between the simulations and the experimental data.

The temperature contours predicted by the ANSYS, Realise 19 [26] 2D formulation employing the proposed 25-species scheme compared against the reference 65-species scheme, are displayed in Fig. 8 depicting three inlet temperature conditions with significant, moderate, and little lift-off from the burner exit. The overall temperature development with the characteristic fishbone structure at the base of the lower lift-off cases and the attendant shift to a tooth-shaped base topology, as we move on to higher lift-offs, have been captured well by the reduced model.

Figure 9 compares the calculated heat release rate fields for the 65-species and 25-species schemes. The shorter 25-species scheme follows the reference scheme rather satisfactorily in all the preheat cases studied. Any deviations observed in the lift-off height are within a 5% margin, whereas the peak heat release rate values display a rather convincing peak deviation of around 5–10% in each case.

Figure 10 shows the $C_2H_2$ concentrations for the two schemes. $C_2H_2$ is an important intermediate hydrocarbon, and its correct representation points to a correct prediction of the main fuel consumption pathways towards lighter hydrocarbons like $CH_4$; it also has a practical significance as a precursor species used for chemiluminescent emission predictions [22]. The lift-off height calculated by the reduced scheme, as already discussed above, depicts minor deviations from the reference model.

Finally, the chemiluminescent emissions of CH* and OH* species of the above-discussed lifted flames are presented in Figs. 11 and 12. Chemiluminescence measurements are a non-intrusive diagnostic tool used in many cases as a heat release rate indicator because this is rather difficult to be measured directly in experiments. As such, it is also critical to be able to assess the flame's chemiluminescent emissions in counterpart simulations. The concentrations of the CH* and OH* species are calculated as follows. In the 65-species scheme, the calculation of the concentrations of CH* and OH* is directly integrated into the kinetic model by incorporating a full chemiluminescence module as presented by Hossain and Nakamura [32]. This approach is computationally demanding in 3D applications and can only be practically realized in laminar flames. In the 25-species scheme, the emissions of CH* and OH* are evaluated through the algebraic model presented by Lytras et al. [22] using a series of precursor species like $C_2H_2$ and O, H, and OH radicals. To assess the accuracy of both methods, the 2D data obtained from the simulations are convoluted to the line of sight projection data [33] in order to be directly comparable to the CH* flame photographs reported by Toma et al. [27].

The convoluted simulation images are presented in Fig. 11 for the two schemes, showing excellent qualitative agreement. Again, a minor deviation between the lift-off heights calculated by the two schemes is apparent, whereas the algebraic model used in conjunction

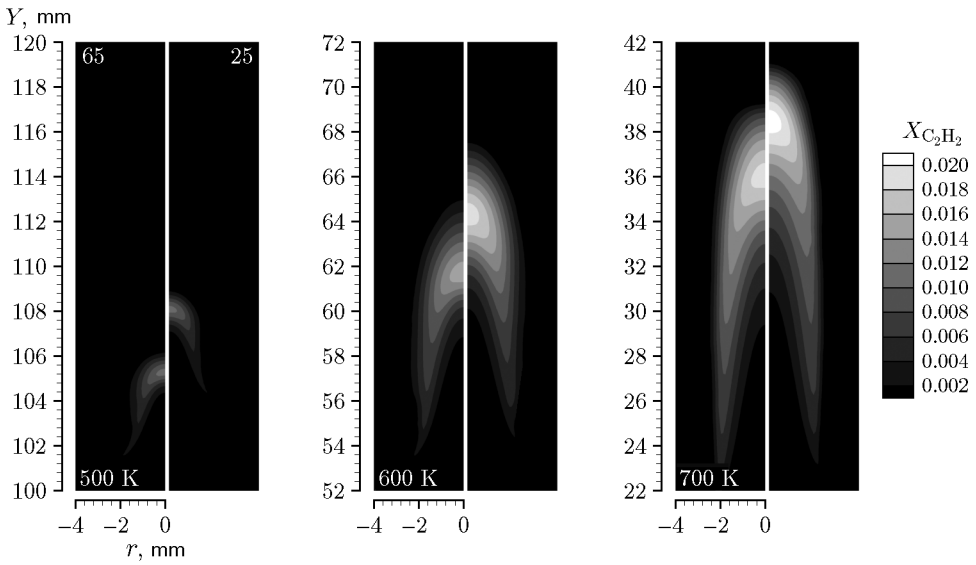


**Fig. 10.** Simulation of the $C_2H_2$ species concentration fields with the reference scheme (65 species) and reduced scheme (25 species) for $T_0 = 500$, 600, and 700 K (the jet velocity is 1.5 m/s, the coflow velocity is 0.4 m/s, and the *n*-heptane mole fraction is 0.035).

with the 25-species scheme to predict the CH* concentrations appears to be in agreement with the direct approach of the 65-species scheme. The 600 K and 700 K cases can also be directly compared against the experimental data [27] showing encouraging promise for the proposed reduced scheme and the use of the algebraic CH* model.

Figure 12 shows the OH* concentrations for the two schemes, each one calculated as discussed above. The two schemes predict the OH* concentration in good agreement for every preheat case.

From the above-described tests and comparisons, it appears that the proposed scheme has an acceptable and consistent behavior over the range of flame conditions investigated and adequately predicts the target characteristics of Section 2. Any inaccuracies that arose due to the species removal process were remedied by employing a pre-exponential factor adjustment in accordance with the prevailing local equivalence ratio, thus, extending the range of applicability of the proposed scheme.

## CONCLUSIONS

An attempt has been made to develop a reduced chemical scheme for high-temperature oxidation of atmospheric *n*-heptane flames. A short skeletal 25-species 69-reaction scheme is presented, which includes a considerable and important section of both the $C_1$ and $C_2$ oxidation routes, meaningful and necessary intermediates, major and minor radicals, as well as a detailed $CO/H_2/O_2$ sub-set. The aim within this shorter reduced scheme is also to avoid rate parameters being expressed in terms of linear algebraic combinations of the excluded elementary step rates.

The chemical rate coefficients of specifically chosen reactions in the reduced schemes were put together as simple Arrhenius expressions, and the optimization process targeted the fine tuning of the pre-exponential constants. All global rates were parametrically calibrated by computing the flame characteristics of well-documented 0D and 1D premixed, freely propagating, and counter-flow jet flames, as well as axisymmetric coflowing laminar lifted (triple) jet flames.

The overall performance of the reduced scheme has been encouraging; with possible enhancements, such as, e.g., addition of an $NO_x$ submodel, this scheme could be suitably included in large-scale 3D turbulent combustion simulations, depending on the affordable computational cost.

While simplified kinetics schemes admittedly do not produce the extent of certain chemical information available with more detailed kinetics, significant features of flame properties are very adequately portrayed. The procedure can be systematically extended to even higher hydrocarbons, e.g., toluene or alternative fuels of technological interest.

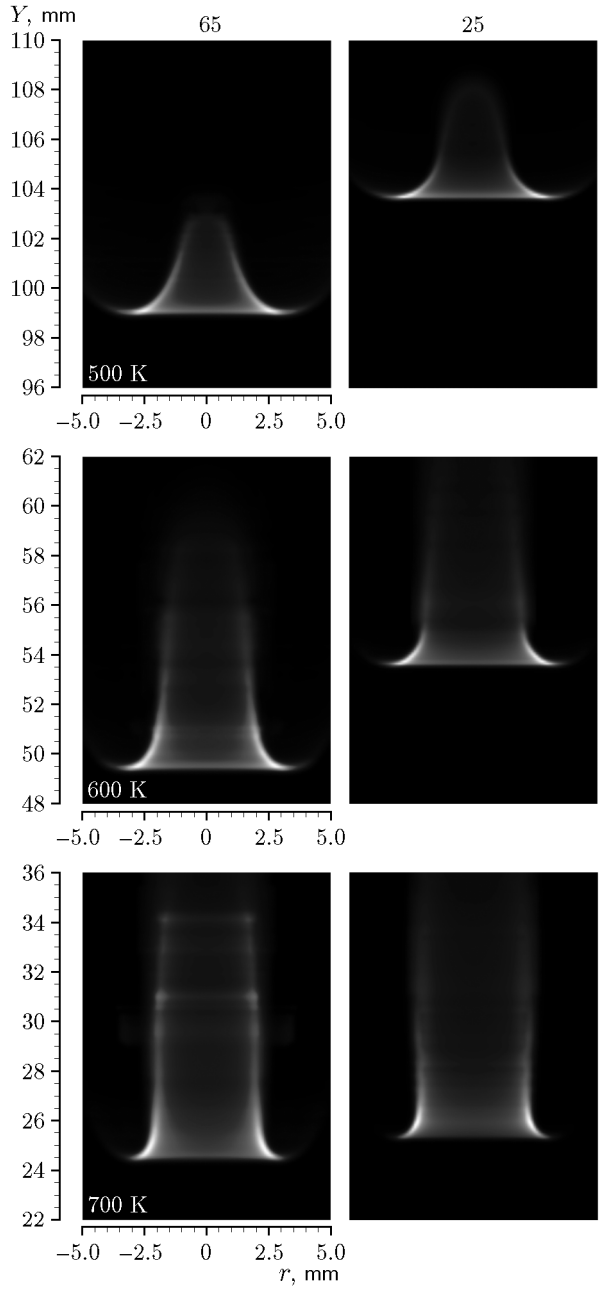


**Fig. 11.** Convoluted simulation images of the CH* concentration with the reference scheme (65 species) and reduced scheme (25 species) for $T_0 = 500$, 600, and 700 K (the jet velocity is 1.5 m/s, the coflow velocity is 0.4 m/s, and the *n*-heptane mole fraction is 0.035).

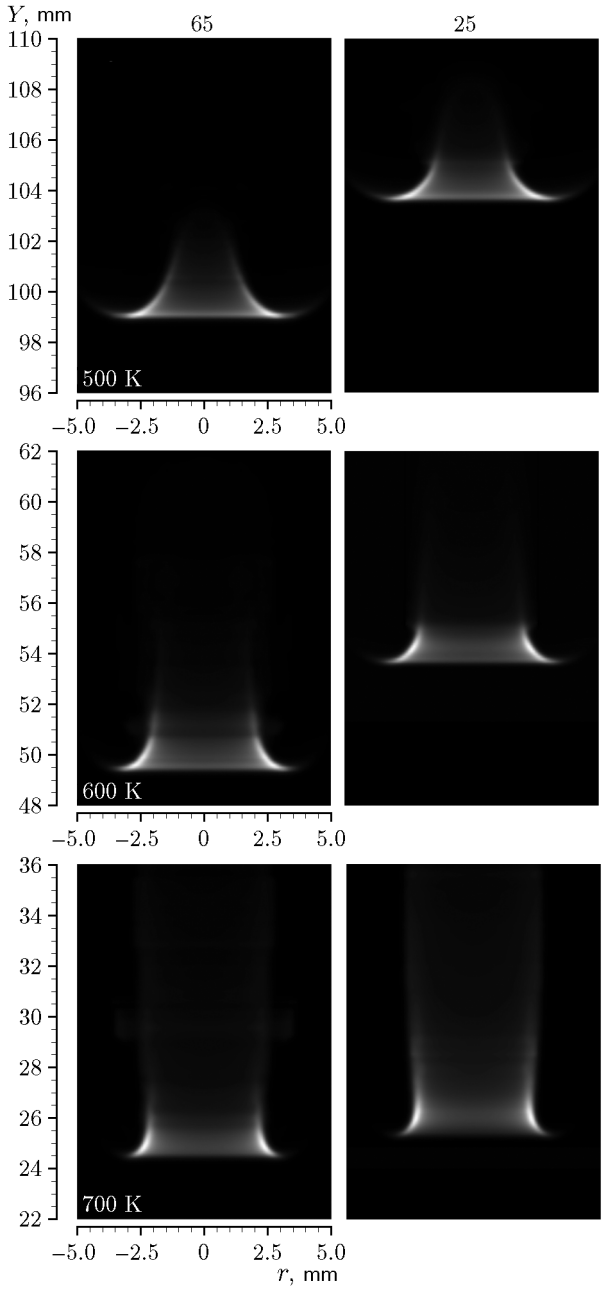


**Fig. 12.** Convoluted simulation images of the OH* concentration with the reference scheme (65 species) and reduced scheme (25 species) for $T_0 = 500$, 600, and 700 K (the jet velocity is 1.5 m/s, the coflow velocity is 0.4 m/s, and the *n*-heptane mole fraction is 0.035).

# APPENDIX

### 25-Species Scheme

ELEMENTS
O H C N
SPECIES
H O OH $HO_2$ $H_2$ $H_2O$ $O_2$ $CH_2$ $CH_2^*$ $CH_3$ $CH_4$ HCO $CH_2O$ CO $CO_2$
$C_2H_2$ $C_2H_3$ $C_2H_4$ $C_2H_5$ *a*-$C_3H_5$ $C_3H_6$ *p*-$C_4H_9$ $NC_7H_{16}$ $SXC_7H_{15}$ $N_2$

| No. | Reaction | $A$, $cm^3$, mol, s | $b$ | $E_a$, cal/mol |
|---|---|---|---|---|
| 1 | $H + O_2 = O + OH$ | $2.64 \cdot 10^{16}$ | $-0.671$ | $1.70 \cdot 10^4$ |
| 2 | $O + H_2 = H + OH$ | $4.59 \cdot 10^4$ | 2.7 | $6.26 \cdot 10^3$ |
| 3 | $OH + H_2 = H + H_2O$ | $1.73 \cdot 10^8$ | 1.51 | $3.43 \cdot 10^3$ |
| 4 | $2OH = O + H_2O$ | $3.97 \cdot 10^4$ | 2.4 | $-2.11 \cdot 10^3$ |
| 5 | $2H + M = H_2 + M$ | $1.78 \cdot 10^{18}$ | $-1$ | $0 \cdot 10^0$ |
| | $H_2/0/H_2O/0/CO_2/0/$ | | | |
| 6 | $2H + H_2O = H_2 + H_2O$ | $5.62 \cdot 10^{19}$ | $-1.25$ | $0 \cdot 10^0$ |
| 7 | $H + OH + M = H_2O + M$ | $4.40 \cdot 10^{22}$ | $-2$ | $0 \cdot 10^0$ |
| | $H_2/2.0/H_2O/6.3/CO/1.75/CO_2/3.6/$ | | | |
| 8 | $O + H + M = OH + M$ | $9.43 \cdot 10^{18}$ | $-1$ | $0 \cdot 10^0$ |
| | $H_2/2.0/H_2O/12.0/CO/1.75/CO_2/3.6/$ | | | |
| 9 | $H + O_2(+M) = HO_2(+M)$ | $5.12 \cdot 10^{12}$ | 0.44 | $0 \cdot 10^0$ |
| | $H_2O/11.89/O_2/0.85/CO/1.09/CO_2/2.18/$<br>LOW / $6.328 \cdot 10^{19}$ $-1.40 \cdot 10^0$ $0 \cdot 10^0$/<br>TROE / $5.0 \cdot 10^{-1}$ $1.00 \cdot 10^{-30}$ $1.0 \cdot 10^{30}$/ | | | |
| 10 | $H_2 + O_2 = HO_2 + H$ | $5.92 \cdot 10^5$ | 2.433 | $5.35 \cdot 10^4$ |
| 11 | $HO_2 + H = O + H_2O$ | $3.97 \cdot 10^{12}$ | 0 | $6.71 \cdot 10^2$ |
| 12 | $HO_2 + H = 2OH$ | $7.49 \cdot 10^{13}$ | 0 | $2.95 \cdot 10^2$ |
| 13 | $HO_2 + O = OH + O_2$ | $4.00 \cdot 10^{13}$ | 0 | $0 \cdot 10^0$ |
| 14 | $HO_2 + OH = O_2 + H_2O$ | $2.38 \cdot 10^{13}$ | 0 | $-5.00 \cdot 10^2$ |
| 15 | $CO + O(+M) = CO_2(+M)$ | $1.36 \cdot 10^{10}$ | 0 | $2.38 \cdot 10^3$ |
| | $H_2/2.0/H_2O/12.0/CO/1.75/CO_2/3.6/$<br>LOW / $1.173 \cdot 10^{24}$ $-2.79 \cdot 10^0$ $4.191 \cdot 10^3$/ | | | |
| 16 | $CO + OH = CO_2 + H$ | $8.00 \cdot 10^{11}$ | 0.14 | $7.35 \cdot 10^3$ |
| 17 | $HCO + H = CO + H_2$ | $1.20 \cdot 10^{14}$ | 0 | $0 \cdot 10^0$ |
| 18 | $HCO + OH = CO + H_2O$ | $3.02 \cdot 10^{13}$ | 0 | $0 \cdot 10^0$ |
| 19 | $HCO + M = CO + H + M$ | $6.50 \cdot 10^{17}$ | $-1$ | $1.70 \cdot 10^4$ |
| | $H_2/2.0/H_2O/0/CO/1.75/CO_2/3.6/$ | | | |
| 20 | $HCO + H_2O = CO + H + H_2O$ | $2.24 \cdot 10^{18}$ | $-1$ | $1.70 \cdot 10^4$ |

**25-Species Scheme (Continued)**

| No. | Reaction | $A$, cm$^3$, mol, s | $b$ | $E_a$, cal/mol |
|---|---|---|---|---|
| 21 | $HCO + O_2 = CO + HO_2$ | $1.20 \cdot 10^9$ | 0.807 | $-7.27 \cdot 10^2$ |
| 22 | $CH_2 + O = HCO + H$ | $8.00 \cdot 10^{13}$ | 0 | $0 \cdot 10^0$ |
| 23 | $CH_2 + OH = CH_2O + H$ | $2.00 \cdot 10^{13}$ | 0 | $0 \cdot 10^0$ |
| 24 | $CH_2 + O_2 = HCO + OH$ | $1.06 \cdot 10^{13}$ | 0 | $1.50 \cdot 10^3$ |
| 25 | $CH_2 + O_2 = CO_2 + 2H$ | $2.64 \cdot 10^{12}$ | 0 | $1.50 \cdot 10^3$ |
| 26 | $CH_2^* + N_2 = CH_2 + N_2$ | $1.50 \cdot 10^{13}$ | 0 | $6.00 \cdot 10^2$ |
| 27 | $CH_2^* + O_2 = H + OH + CO$ | $2.80 \cdot 10^{13}$ | 0 | $0 \cdot 10^0$ |
| 28 | $CH_2^* + O_2 = CO + H_2O$ | $1.20 \cdot 10^{13}$ | 0 | $0 \cdot 10^0$ |
| 29 | $CH_2^* + H_2O = CH_2 + H_2O$ | $3.00 \cdot 10^{13}$ | 0 | $0 \cdot 10^0$ |
| 30 | $CH_2^* + CO = CH_2 + CO$ | $9.00 \cdot 10^{12}$ | 0 | $0 \cdot 10^0$ |
| 31 | $CH_2O + H = HCO + H_2$ | $2.30 \cdot 10^9$ | 1.05 | $3.28 \cdot 10^3$ |
| 32 | $CH_2O + O = HCO + OH$ | $3.90 \cdot 10^{13}$ | 0 | $3.54 \cdot 10^3$ |
| 33 | $CH_2O + OH = HCO + H_2O$ | $3.43 \cdot 10^9$ | 1.18 | $-4.47 \cdot 10^2$ |
| 34 | $CH_3 + H(+M) = CH_4(+M)$ | $1.27 \cdot 10^{16}$ | $-0.63$ | $3.83 \cdot 10^2$ |
| | $H_2$/2.0/$H_2O$/6.0/$CH_4$/2.0/CO/1.5/$CO_2$/2.0/<br>LOW / $2.477 \cdot 10^{33}$ $-4.76 \cdot 10^0$ $2.44 \cdot 10^3$/<br>TROE / $7.83 \cdot 10^{-1}$ $7.40 \cdot 10^1$ $2.94 \cdot 10^3$ | | | |
| 35 | $CH_3 + O = CH_2O + H$ | $8.43 \cdot 10^{13}$ | 0 | $0 \cdot 10^0$ |
| 36 | $CH_3 + OH = CH_2 + H_2O$ | $5.60 \cdot 10^7$ | 1.6 | $5.42 \cdot 10^3$ |
| 37 | $CH_3 + OH = CH_2^* + H_2O$ | $2.50 \cdot 10^{13}$ | 0 | $0 \cdot 10^0$ |
| 38 | $2CH_3 = H + C_2H_5$ | $4.99 \cdot 10^{12}$ | 0.1 | $1.06 \cdot 10^4$ |
| 39 | $CH_4 + O = CH_3 + OH$ | $1.02 \cdot 10^9$ | 1.5 | $8.60 \cdot 10^3$ |
| 40 | $CH_4 + OH = CH_3 + H_2O$ | $8.50 \cdot 10^8$ | 1.6 | $3.12 \cdot 10^3$ |
| 41 | $C_2H_3(+M) = C_2H_2 + H(+M)$ | $3.86 \cdot 10^8$ | 1.62 | $3.70 \cdot 10^4$ |
| | $H_2$/2.0/$H_2O$/6.0/$CH_4$/2.0/CO/1.5/$CO_2$/2.0/$C_2H_2$/3.0/$C_2H_4$/3.0/<br>LOW / $2.565 \cdot 10^{27}$ $-3.40 \cdot 10^0$ $3.579872 \cdot 10^4$/<br>TROE / $1.9816 \cdot 10^0$ $5.38 \cdot 10^3$ $4.30 \cdot 10^0$ | | | |
| 42 | $C_2H_2 + O = CH_2 + CO$ | $7.50 \cdot 10^7$ | 2 | $1.90 \cdot 10^3$ |
| 43 | $C_2H_3 + H = C_2H_2 + H_2$ | $7.00 \cdot 10^{14}$ | 0 | $0 \cdot 10^0$ |
| 44 | $C_2H_3 + O = CH_3 + CO$ | $4.80 \cdot 10^{13}$ | 0 | $0 \cdot 10^0$ |
| 45 | $C_2H_3 + OH = C_2H_2 + H_2O$ | $3.01 \cdot 10^{13}$ | 0 | $0 \cdot 10^0$ |
| 46 | $C_2H_3 + O_2 = HCO + CH_2O$ | $4.60 \cdot 10^{16}$ | $-1.39$ | $1.01 \cdot 10^3$ |
| 47 | $C_2H_4 + H(+M) = C_2H_5(+M)$ | $1.37 \cdot 10^9$ | 1.463 | $1.36 \cdot 10^3$ |
| | LOW / $2.027 \cdot 10^{39}$ $-6.64 \cdot 10^0$ $5.769 \cdot 10^3$/<br>TROE / $-5.69 \cdot 10^{-1}$ $2.99 \cdot 10^2$ $9.15 \cdot 10^3$ | | | |

**25-Species Scheme (Continued)**

| No. | Reaction | $A$, cm$^3$, mol, s | $b$ | $E_a$, cal/mol |
|---|---|---|---|---|
| 48 | $C_2H_4 + H = C_2H_3 + H_2$ | $5.07 \cdot 10^7$ | 1.9 | $1.30 \cdot 10^4$ |
| 49 | $C_2H_4 + O = C_2H_3 + OH$ | $1.51 \cdot 10^7$ | 1.9 | $3.74 \cdot 10^3$ |
| 50 | $C_2H_4 + O = CH_3 + HCO$ | $8.92 \cdot 10^5$ | 1.83 | $2.20 \cdot 10^2$ |
| 51 | $C_2H_4 + O = CH_2 + CH_2O$ | $3.84 \cdot 10^5$ | 1.83 | $2.20 \cdot 10^2$ |
| 52 | $C_2H_4 + OH = C_2H_3 + H_2O$ | $3.60 \cdot 10^6$ | 2 | $2.50 \cdot 10^3$ |
| 53 | $C_2H_5 + H = C_2H_4 + H_2$ | $2.00 \cdot 10^{13}$ | 0 | $0 \cdot 10^0$ |
| 54 | $C_2H_5 + O = CH_3 + CH_2O$ | $1.60 \cdot 10^{13}$ | 0 | $0 \cdot 10^0$ |
| 55 | $C_2H_5 + O_2 = C_2H_4 + HO_2$ | $2.00 \cdot 10^{10}$ | 0 | $0 \cdot 10^0$ |
| 56 | $C_2H_5 + HO_2 = CH_3 + CH_2O + OH$ | $2.40 \cdot 10^{13}$ | 0 | $0 \cdot 10^0$ |
| 57 | $a$-$C_3H_5 + H(+M) = C_3H_6(+M)$ | $2.00 \cdot 10^{14}$ | 0 | $0 \cdot 10^0$ |
| | $H_2$/2.0/$H_2O$/6.0/$CH_4$/2.0/CO/1.5/$CO_2$/2.0/<br>LOW / $1.33 \cdot 10^{60}$ $-1.20 \cdot 10^1$ $5.9678 \cdot 10^3$/<br>TROE / $2.0 \cdot 10^{-2}$ $1.10 \cdot 10^3$ $1.10 \cdot 10^3$ | | | |
| 58 | $a$-$C_3H_5 + HO_2 = OH + C_2H_3 + CH_2O$ | $6.60 \cdot 10^{12}$ | 0 | $0 \cdot 10^0$ |
| 59 | $C_3H_6 + H = C_2H_4 + CH_3$ | $2.00 \cdot 10^{22}$ | $-2.39$ | $1.12 \cdot 10^4$ |
| 60 | $C_3H_6 + H = a$-$C_3H_5 + H_2$ | $8.50 \cdot 10^4$ | 2.5 | $2.49 \cdot 10^3$ |
| 61 | $C_3H_6 + O = C_2H_5 + HCO$ | $3.50 \cdot 10^7$ | 1.65 | $-9.72 \cdot 10^2$ |
| 62 | $C_3H_6 + O = a$-$C_3H_5 + OH$ | $1.80 \cdot 10^{11}$ | 0.7 | $5.88 \cdot 10^3$ |
| 63 | $C_3H_6 + OH = a$-$C_3H_5 + H_2O$ | $9.10 \cdot 10^5$ | 2 | $-2.98 \cdot 10^2$ |
| 64 | $C_2H_4 + C_2H_5 = p$-$C_4H_9$ | $1.50 \cdot 10^{11}$ | 0 | $7.30 \cdot 10^3$ |
| 65 | $p$-$C_4H_9 + C_3H_6 = SXC_7H_{15}$ | $3.00 \cdot 10^{12}$ | 0 | $7.30 \cdot 10^3$ |
| 66 | $NC_7H_{16} + H = SXC_7H_{15} + H_2$ | $1.25 \cdot 10^6$ | 2.4 | $4.47 \cdot 10^3$ |
| 67 | $NC_7H_{16} + O = SXC_7H_{15} + OH$ | $5.52 \cdot 10^5$ | 2.71 | $2.11 \cdot 10^3$ |
| 68 | $NC_7H_{16} + OH = SXC_7H_{15} + H_2O$ | $5.40 \cdot 10^4$ | 2.39 | $3.93 \cdot 10^2$ |
| 69 | $NC_7H_{16} + O_2 = SXC_7H_{15} + HO_2$ | $8.00 \cdot 10^{13}$ | 0 | $4.76 \cdot 10^4$ |

## REFERENCES


1. K. Luo, H. Pitsch, M. G. Pai, and O. Desjardins, "Direct Numerical Simulations and Analysis of Three-Dimensional $n$-heptane Spray Flames in a Model Swirl Combustor," Proc. Combust. Inst. **33** (2), 2143–2152 (2011); DOI: 10.1016/j.proci.2010.06.077.
2. H. Larabi, G. Lartigue, and V. Moureau, "LES Study of an $n$-heptane/air Turbulent Spray Jet Flame," in *2018 AIAA Aerospace Sciences Meeting*; DOI: 10.2514/6.2018-0500.
3. Z. Li, M. J. Evans, J. Ye, et al., "Numerical and Experimental Investigation of Turbulent $n$-Heptane Jet-in-Hot-Coflow Flames," Fuel **283**, 118748 (2021); DOI: 10.1016/j.fuel.2020.118748.
4. S. Gallot-Lavallée and W. P. Jones, "Large Eddy Simulation of Spray Auto-Ignition under EGR Conditions," Flow, Turbul. Combust. **96** (2), 513–534 (2016).
5. F. L. Sacomano Filho, G. Kuenne, M. Chrigui, et al., "A Consistent Artificially Thickened Flame Approach for Spray Combustion Using LES and the FGM Chemistry Reduction Method: Validation in Lean Partially Pre-Vaporized Flames," Combust. Flame **184**, 68–89 (2017); DOI: 10.1016/j.combustflame.2017.05.031.
6. T. Lu and C. K. Law, "Strategies for Mechanism Reduction for Large Hydrocarbons: $n$-Heptane," Combust. Flame **154** (1/2), 153–163 (2008); DOI: 10.1016/j.combustflame.2007.11.013.
7. L. Seidel, K. Moshammer, X. Wang, et al., "Comprehensive Kinetic Modeling and Experimental Study of a Fuel-Rich, Premixed $n$-Heptane Flame," Combust. Flame **162** (5), 2045–2058 (2015); DOI: 10.1016/j.combustflame.2015.01.002.
8. S. Voglsam and F. Winter, "A Global Combustion Model for Simulation of $n$-Heptane and Iso-Octane Self Ignition," Chem. Eng. J. **203**, 357–369 (2012); DOI: 10.1016/j.cej.2012.06.086.
9. K. E. Niemeyer, C.-J. Sung, and M. P. Raju, "Skeletal Mechanism Generation for Surrogate Fuels Using Directed Relation Graph with Error Propagation and Sensitivity Analysis," Combust. Flame **157** (9), 1760–1770 (2010); DOI: 10.1016/j.combustflame.2009.12.022.
10. H. Wang, X. You, A. V. Joshi, et al., *USC Mech Version II. High-Temperature Combustion Reaction Model of* $H_2/CO/C_1$–$C_4$ *Compounds* (2007); http://ignis.usc.edu/USC Mech II.htm.
11. C. S. Yoo, T. Lu, J. H. Chen, and C. K. Law, "Direct Numerical Simulations of Ignition of a Lean $n$-Heptane/air Mixture with Temperature Inhomogeneities at Constant Volume: Parametric Study," Combust. Flame **158** (9), 1727–1741 (2011); DOI: 10.1016/j.combustflame.2011.01.025.
12. N. Peters and F. A. Williams, "The Asymptotic Structure of Stoichiometric Methane–Air Flames," Combust. Flame **68** (2), 185–207 (1987); DOI: 10.1016/0010-2180(87)90057-5.
13. A. Arvidsson, *Development of an Automatic Reduction Tool for Chemical Mechanisms and an Optimized Sparse Matrix Solver for Systems of Differential and Algebraic Equations* (Lund Univ., 2010).
14. C. Pichler and E. J. K. Nilsson, "Analysis of Important Chemical Pathways of $n$-Heptane Combustion in Small Skeletal Mechanisms," Energy Fuels **34** (1), 758–768 (2020); DOI: 10.1021/acs.energyfuels.9b03263.
15. J. Zheng, D. Miller, and N. P. Cernansky, "A Global Reaction Model for the HCCI Combustion Process," SAE Tech. Papers (2004); DOI: 10.4271/2004-01-2950.
16. A. J. Smallbone, W. Liu, C. K. Law, et al., "Experimental and Modeling Study of Laminar Flame Speed and Non-Premixed Counterflow Ignition of $n$-Heptane," Proc. Combust. Inst. **32** (1), 1245–1252 (2009); DOI: 10.1016/j.proci.2008.06.213.
17. M. Mehl, W. J. Pitz, C. K. Westbrook, and H. J. Curran, "Kinetic Modeling of Gasoline Surrogate Components and Mixtures under Engine Conditions," Proc. Combust. Inst. **33** (1), 193–200 (2011); DOI: 10.1016/j.proci.2010.05.027.
18. M. Sarathy, N. Atef, A. Alfazazi, et al., "Reduced Gasoline Surrogate (Toluene/$n$-Heptane/Iso-octane) Chemical Kinetic Model for Compression Ignition Simulations," SAE Int. (2018); DOI: 10.4271/2018-01-0191.
19. G. Paterakis, E. Politi, and P. Koutmos, "Experimental Investigation of Isothermal Scalar Mixing Fields Downstream of Axisymmetric Baffles under Fully Premixed or Stratified Inlet Mixture Conditions," Exp. Therm. Fluid Sci. **108**, 1–15 (2019); DOI: 10.1016/j.expthermflusci.2019.05.018.
20. K. Souflas, K. Perrakis, and P. Koutmos, "On the Turbulent Flow and Pollutant Emission Characteristics of Disk Stabilized Propane–Air Flames, under Inlet Mixture Stratification and Preheat," Fuel **260**, 116333 (2020); DOI: 10.1016/j.fuel.2019.116333.
21. "Chemkin 19.0, Reaction Design" (2018).
22. I. Lytras, E. P. Mitsopoulos, E. Dogkas, and P. Koutmos, "Algebraic Model for Chemiluminescence Emissions Suitable for Using in Complex Turbulent Propane Flame Simulations," Fiz. Goreniya Vzryva **56** (3), 36–50 (2020) [Combust., Expl., Shock Waves **56** (3), 278–291 (2020)]; DOI: 10.1134/S0010508220030041.
23. M. J. Dunn, "Finite-Rate Chemistry Effects in Turbulent Premixed Combustion," Univ. of Sydney (2008).
24. E. P. Mitsopoulos, I. Lytras, and P. Koutmos, "Large Eddy Simulations of Premixed $CH_4$ Bluff-Body Flames Operating Close to the Lean Limit Using Quasi-Global Chemistry and an Algebraic Chemiluminescence Model," Theor. Comput. Fluid Dyn. **33** (3), 325–340 (2019).

25. P. Gokulakrishnan et al., "Reduced Kinetic Mechanism for Reactive Flow Simulation of Syngas/Methane Combustion at Gas Turbine Conditions," in *ASME Turbo Expo 2006: Power for Land, Sea, and Air* (2006), pp. 513–521; DOI: 10.1115/GT2006-90573.
26. "ANSYS®Academic Research, Release 19" (2018).
27. M. Toma, F. Bisetti, S. M. Sarathy, et al., "Numerical Simulation of Lifted Tribrachial *n*-Heptane Laminar Flames in Heated Coflow," in *Proc. of the 6th Eur. Combust. Meeting* (Sweden, 2013).
28. H. K. Ciezki and G. Adomeit, "Shock-Tube Investigation of Self-Ignition of *n*-Heptane–Air Mixtures under Engine Relevant Conditions," Combust. Flame **93** (4), 421–433 (1993); DOI: 10.1016/0010-2180(93)90142-P.
29. C. Ji, E. Dames, Y. L. Wang, et al., "Propagation and Extinction of Premixed $C_5$–$C_{12}$ *n*-Alkane Flames," Combust. Flame **157** (2), 277–287 (2010); DOI: 10.1016/j.combustflame.2009.06.011.
30. Z. Cheng, R. W. Pitz, and J. A. Wehrmeyer, "Lean and Ultralean Stretched Propane–Air Counterflow Flames," Combust. Flame **145** (4), 647–662 (2006); DOI: 10.1016/j.combustflame.2006.02.006.
31. E. Dogkas, I. Lytras, P. Koutmos, and G. Kontogouris, "Reduced Kinetic Schemes for Complex Reacting Flow Computations of Propane–Air Combustion," Fiz. Goreniya Vzryva **56** (1), 27–41 (2020) [Combust., Expl., Shock Waves 56 (1), 23–35 (2006)]; DOI: 10.1134/S0010508220030041.
32. A. Hossain and Y. Nakamura, "A Numerical Study on the Ability to Predict the Heat Release Rate Using CH* Chemiluminescence in Non-Sooting Counterflow Diffusion Flames," Combust. Flame **161** (1), 162–172 (2014); DOI: 10.1016/j.combustflame.2013.08.021.
33. K. M. Martin, *Acoustic Modification of Sooting Combustion* (Univ. of Texas at Austin, 2002).